Earth Planet. Sci. Lett. 691 (2026) 120220

Contents lists available at ScienceDirect

Earth and Planetary Science Letters

journal homepage: www.elsevier.com/locate/epsl

Coevolution between crustal thickness and sulfur oxidation state in Gangdese felsic magmas

Xuyang Zheng *, Ming Tang, Hao Chen, Ziyi Guo

SKLab-DeepMinE, MOEKLab-OBCE, School of Earth and Space Sciences, Peking University, Beijing, 100871, China

ARTICLE INFO

Edited by: Dr Fang-Zhen Teng

Keywords:
Detrital zircon-hosted apatite Sulfur oxidation state Felsic magmas Porphyry copper deposits Gangdese Belt

ABSTRACT

Whether the abundant sulfate (S^{6+}) of oxidized felsic magmas at convergent plate margins is sourced from subducted materials or generated through magmatic differentiation remains poorly understood. Here, we use S content in apatite to track the evolution of S redox state in felsic magmas over the past ~120 Myr in the eastern Gangdese, southern Tibet. Unlike previous studies that rely on apatite grains separated from igneous rocks, we measure S in apatite inclusions hosted in detrital zircon. This approach enables us to assess magmatic S oxidation across the orogenic crust on a significantly broader scale than permitted by limited rock samples. Our results show two episodes of systematically elevated apatite S contents in the eastern Gangdese: one during the Late Cretaceous (95-80 Ma) and another from the Late Paleocene to the Miocene (45-10 Ma), following the India-Eurasia collision. This apatite S trend is consistent with that of the magma fO_2 reconstructed using zircon Ce-U-Ti oxybarometer. More importantly, both apatite S content and magma fO_2, on average, correlate with crustal thickness. While source composition and assimilation processes may contribute to redox heterogeneity in felsic magmas, our findings point to the critical role of crustal thickness in modulating the oxidation state of felsic magmas on an orogenic scale. Finally, by tracing oxidized S through detrital zircon samples, which are easy to collect and analytically efficient, our approach may allow for quick and effective evaluation of regional potential for porphyry copper mineralization.

1. Introduction

Porphyry copper deposits (PCDs) supply >70% of global economic Cu and are closely associated with intermediate-felsic magmatic intrusions emplaced in thickened magmatic arcs (Richards, 2021; Sillitoe, 2010). One notable characteristic of these magmas is their high sulfate contents (Chambefort et al., 2008; Grondahl and Zajacz, 2022; Meng et al., 2022; Park et al., 2021), and many of them are saturated with anhydrite (Audétat et al., 2025a, b; Chang et al., 2018; Hutchinson and Dilles, 2019). Sulfur oxidation suppresses extensive sulfide crystallization in upper crustal magma chambers, so that Cu can be more efficiently extracted by exsolving fluids during magmatic-hydrothermal transition (Richards, 2015). To convert sulfide to sulfate in felsic magmas, the magmas need to be sufficiently oxidized, and these strongly oxidized magmas typically form at convergent margins (Lee and Tang, 2020; Richards, 2021; Sillitoe, 2010).

However, not all felsic magmas at convergent margins are oxidized (Loucks et al., 2024), and the factors controlling the redox state of felsic magmas remain not fully understood. This problem differs from that of the oxidation of basaltic arc magmas, which is usually attributed to fluids or partial melts derived from subducting slabs containing carbonates, sulfate, and/or magnetite (Beaudry and Sverjensky, 2024; Evans, 2012; Kelley and Cottrell, 2009; Muth and Wallace, 2022). Felsic magmas typically form through extensive magmatic differentiation of basaltic precursors (Annen et al., 2006), whose redox signatures may become less relevant to basaltic magmas because differentiation significantly changes the composition of magmas. Recent studies suggest that fractionation of Fe^{2+}-rich minerals (e.g. garnet, amphibole) in the deep lower crust can effectively remove Fe^{2+} from the melt, thus elevating $Fe^{3+}/\Sigma Fe$ of residual magmas and driving endogenic oxidation (Luo et al., 2024; Tang et al., 2018). These new findings point to intracrustal petrological processes playing an important role in controlling the redox state of felsic magmas, which in turn determines the redox state of S in the melts.

The S redox state in the melt can be constrained by measuring S content in apatite, because S partitioning in apatite is highly dependent on the oxidation state of S in the silicate melt (Konecke et al., 2019; Parat et al., 2011; Peng et al., 1997). In reduced melts where S is dominated by

* Corresponding author.
E-mail address: xuyangzheng@stu.pku.edu.cn (X. Zheng).

https://doi.org/10.1016/j.epsl.2026.120220
Received 25 November 2025; Received in revised form 18 June 2026; Accepted 1 July 2026
Available online 13 July 2026
0012-821X/© 2026 Elsevier B.V. All rights are reserved, including those for text and data mining, AI training, and similar technologies.

S^{2-}, apatite incorporates little S (less than a few hundred ppm) because S^{2-} is incompatible in apatite (Konecke et al., 2019). By contrast, under oxidizing conditions, S is mainly present as SO_4^{2-}, which is readily incorporated into apatite and yields elevated S concentrations (>1000 ppm) (Konecke et al., 2019; Konecke et al., 2017; Peng et al., 1997). Tang et al. (2020) measured S content in apatite separated from granitoids in the Gangdese batholith. In combination with whole-rock Dy/Yb ratios, Tang et al. (2020) suggested that sulfur oxidation in felsic magmas is closely related to fractionation of garnet induced by crustal thickening. But it is unclear whether their limited rock samples (n = 21) can fully capture the magmatic evolution of the extensive Gangdese Belt over >100 Myr.

Here, for the first time, we combine S-in-apatite with the detrital zircon records to trace magmatic S oxidation, which provides broader spatial and temporal coverage of magmatism in the Gangdese Belt. We measured S in apatite inclusions within detrital zircons and reconstructed the evolution of magmatic S oxidation state from the early Cretaceous to the Miocene. Unlike apatites separated from rocks, these zircon-hosted apatites are shielded from metasomatism, recrystallization and hydrothermal re-equilibration, thereby better preserving primary magmatic signatures (Nathwani et al., 2023; Wang et al., 2025a). Their ages can also be constrained by U-Pb dating of the host zircons, which provide a more robust age constraints than direct apatite dating. Additionally, we applied zircon Ce-Ti-U oxybarometer to track the evolution of magma oxygen fugacity. These trends were then compared with the evolution of crustal thickness and the redox state of the primitive basaltic magmas. The results allow us to evaluate the contributions of oxidized material in the source vs. magmatic differentiation to the oxidation of felsic magmas, thereby inferring the oxidation pathway of felsic magmas. Finally, we discussed the implications for the formation and exploration of PCDs in magmatic orogens.

2. Geological background and samples

The Tibetan Plateau comprises a series of accreted terranes, from south to north: the Himalayas, Lhasa, Qiangtang, Songpan-Ganze, and Kunlun terranes (Yin and Harrison, 2000). Situated along the southern margin of the Lhasa Terrane, the Gangdese Belt is one of the most strongly thickened continental arcs on Earth, with crustal thickness exceeding 60 km since the Eocene (Zhu et al., 2023). This belt records the entire history of Neo-Tethyan Ocean closure and India-Eurasia collision (Allegre et al., 1984). The prolonged tectonism has been accompanied by long-lived magmatic activity from Triassic to the present, which has led to the formation of the extensive Gangdese Batholith spanning over 1500 km along the India-Eurasia suture zone (Zhu et al., 2023). The batholith is more deeply eroded in the east due to the indentation of the Indian plate along the eastern Himalayan syntaxis (Cao et al., 2020).

The Gangdese Belt hosts a cluster of giant PCDs (e.g., Qulong and Jiama) aligned along the southern margin of the Lhasa Terrane, representing one of the most significant porphyry copper districts in Asia (Hou et al., 2015). These PCDs occur mainly along a ~200 km E-W corridor in the eastern Gangdese and predominantly situated in the post-collisional intrusions at shallow crustal levels, with mineralization ages predominantly ranging from 20 to 10 Ma (Hou et al., 2015; Wang et al., 2015b).

In this study, we collected river sands from eight modern rivers draining the eastern Gangdese (~90°E to ~95°E, Fig. 1), where large to giant PCDs were formed. Catchment analysis confirms that the drainage areas of our river sand samples cover most of the eastern Gangdese while excluding the Himalayas sources. Detrital zircon grains were separated from the river sands for geochronology and trace element analysis through laser ablation-inductively coupled plasma–mass spectrometry (LA-ICP-MS). Major element analysis of zircon-hosted apatite were done through electron probe microanalysis (EPMA).

3. Analytic methods

3.1. Zircon U-Pb dating and trace elements analysis

Zircon grains separated from the river sands were analyzed for their U-Pb isotopes and trace elements simultaneously at the HR-IDEA Lab at Peking University. Analyses were conducted using an Element 2 sector field-inductively coupled plasma-mass spectrometer coupled to a ESI New Wave NWR 193UC (Two Vol2) laser ablation system. Helium was used as carrier gas to reduce melting at the laser pit and generate small and uniform particles. Before each analytical session, we optimized the instrument to obtain high sensitivities while maintaining low oxide yield

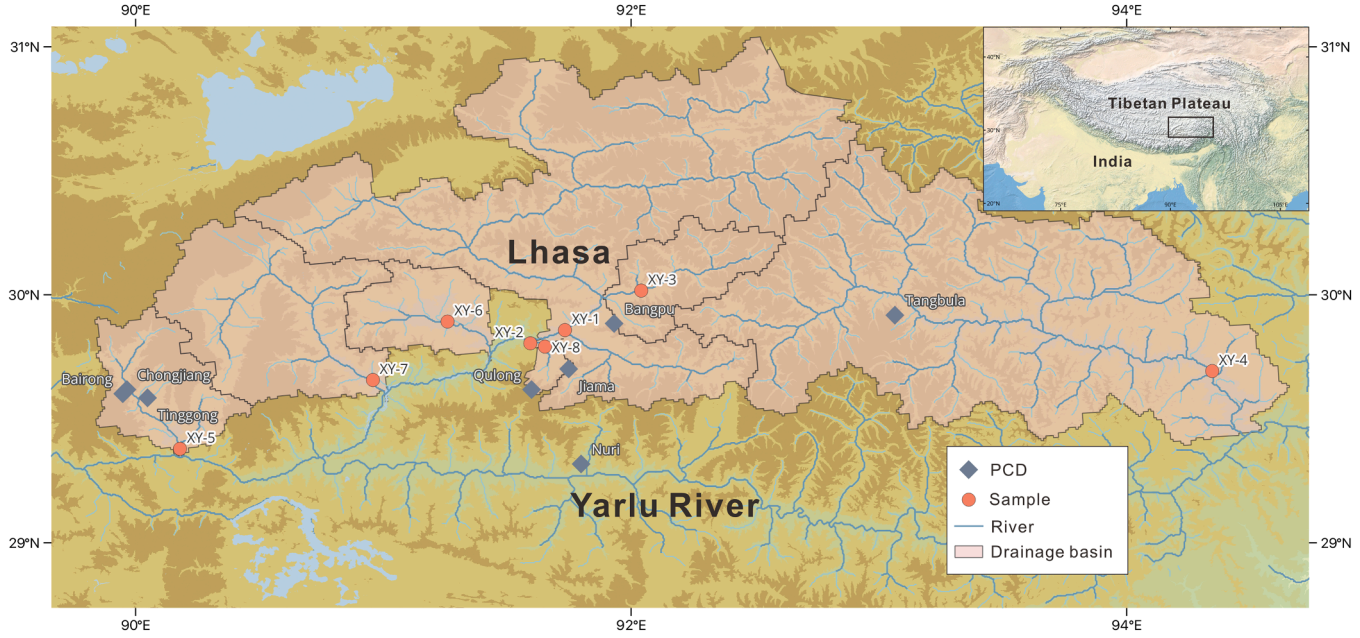


Fig. 1. Map showing the sampling sites, drainage areas of each river sand sample, names and locations of major PCDs in the eastern Gangdese. The geographic coordinates of the samples are available in the Supplementary Material (Table. S1).

($^{232}Th^{16}O^{+}/^{232}Th^{+} \leq 0.2\%$).

All analyses were conducted with a 25 μm diameter beam size, ~3 J/cm^2 laser fluence, and 5 Hz repetition rate. To minimize possible age discrepancies, we selected zircon spots adjacent to apatite inclusions and within the same zircon growth zones as the inclusions. Each analysis comprised 40 s background signal collection followed by 60 s zircon data collection. For U-Pb age determination, we used zircon 91500 as the external standard and zircon SA01 as the monitor standard for U-Pb dating. For trace elements measurements, andesitic glass ARM-3 was used as the external reference material with ^{29}Si serving as the internal standard. The sample standard bracketing method was used in which zircon 91500 and ARM-3 were measured twice before and after 10 sample analyses. Repeated analyses of zircon SA01 yielded a mean $^{206}Pb/^{238}U$ age of 534.0 ± 1.7 Ma (2 SE) and Eu/Eu* of 1.09 ± 0.11 (2 SD) (Fig. S1 and S2). These measured age and Eu/Eu* are consistent with the recommended values (Huang et al., 2019).

3.2. Apatite sulfur contents

Apatite S contents were measured by electron probe microanalysis, which was performed on a JEOL JXA-8230 at Peking University. We used spot mode, set the voltage at 15 kV and used a 50 nA current to increase S counting statistics and lower the detection limit of S. The on-peak and background counting times were 20 s and 5 s for Ca; 20 s and 15 s for P; 10 s and 5 s for Si, respectively. Longer counting times were used for S, Cl and F: 60 s per peak and 30 s per each background. Sulfur was analyzed in differential mode, in order to avoid interferences with secondary X-rays from trace REE. And a large and sensitive PETH analyzing crystal was used for S analysis, in order to improve the X-ray intensity. The standards employed for element calibration were natural minerals: Durango apatite for P and F, jadeite for Si, SPI apatite for Ca, SPI anhydrite for S, and SPI tugtupite for Cl. The PhiRoZ (JEOL) matrix correction was employed for quantification. It should be noted that, while the high beam current is optimal for S analysis, it inevitably induces significant F migration in apatite (Stormer et al., 1993), leading to overestimation of F contents. In addition, due to the extremely small size of apatite inclusions (<10 μm), some analyses were affected by contamination from the host zircon, which can result in elevated SiO_2 contents. We removed the data with SiO_2 content > 5%.

4. Results

4.1. Zircon geochronology, crustal thickness, and magmatic oxygen fugacity

We measured U-Pb ages and trace element for 949 detrital zircon grains. To enhance data density, an additional 1,636 detrital zircon analyses from four samples reported by Tang et al. (2021) were incorporated for the calculation of crustal thickness. The data were binned into 5 Myr intervals. The bulk zircon age distribution (Fig. S6) shows three prominent peaks at 90-80 Ma, 70-45 Ma, 25-10 Ma, aligning well with the distribution of crystallization ages of intrusive rock samples reported by Ji et al. (2009) and Zhu et al. (2023). This consistency indicates that the detrital samples are representative of magmatism in the eastern Gangdese.

We employed the empirical relationship between crustal thickness and zircon Eu anomaly (Tang et al., 2021) to calculate crustal thickness. Following the filtering criteria proposed by Tang et al. (2024a), we excluded zircon analyses with La > 1 ppm, Eu/Eu* > 1, Th/U ratio < 0.1, and P > 750 ppm to eliminate data compromised by mineral inclusions, metamorphic alteration, and zircon grains from S-type granites. These filtering procedures reduce the dataset by ~16.7%, leaving 2,153 data points. For comparison, we also calculated crustal thickness based on the empirical relationship between crustal thickness and whole-rock La/Yb ratio (Profeta et al., 2015). The whole-rock data are sourced from Tibetan magmatism database (Chapman and Kapp, 2017) and are restricted to intermediate-felsic rocks with SiO_2 contents of 55-70 wt%. The crustal thicknesses reconstructed from detrital zircon Eu/Eu* and whole rock La/Yb show consistent patterns. Both proxies indicate two episodes of crustal thickening in the eastern Gangdese over the past 120 Myr (Fig. 2C and 2D). The first episode took place between 100-80 Ma, when the crust thickened from ~40 km to ~60 km; the more recent episode started at ~50 Ma, when the crust thickened from 40-50 km to >60 km.

Using the 949 zircon analyses reported in this study, and following the same filtering criteria used for the calculation of crustal thickness, we calculated magmatic fO_2 using the zircon Ce-Ti-U oxybarometer (Loucks et al., 2020). The results show that magmatic fO_2 increases from ΔFMQ ≈ 0 to > +1.0 between 100 and 80 Ma, then decreases and becomes relatively stable from 80 to 60 Ma, and rises sharply again to ΔFMQ > +1.5 between 55 and 40 Ma, after which it remains largely constant.

4.2. Sulfur contents in apatite inclusions hosted in detrital zircons

We measured S contents for 472 zircon-hosted apatite inclusions. The data were also binned into 5 Myr intervals. The apatite S content exhibits a multi-stage evolution (Fig. 2A), characterized by a gradual increase from ~100 to ~700 ppm between 100 and 80 Ma, a subsequent decline to ~130 ppm by 65 Ma, and a rapid rise to >1500 ppm by 45 Ma, remaining high (1200–2000 ppm) thereafter.

5. Discussion

5.1. Crustal thickening in the eastern Gangdese

Detrital zircon Eu/Eu* and whole-rock La/Yb ratio reveal two episodes of crustal thickening: one during the Late Cretaceous and another from ~55 Ma to the Miocene, consistent with several previous studies (e.g., Ji et al. (2014); Tang et al. (2021)). But it is debated whether the Gangdese crust was thickened between 90-80 Ma. Zhu et al. (2017) proposed that the high-pressure differentiation signatures of the Late Cretaceous samples resulted from oceanic crust melting instead of crustal thickening. Nevertheless, a Late Cretaceous thickening scenario is more consistent with several lines of regional geological evidence, such as progressive burial from 20 km to 40 km in eastern Gangdese (Cao et al., 2020), and rapid N-S shortening in Lhasa terrane (Leier et al., 2007). Paleoelevation estimates from triple oxygen isotopes (Ibarra et al., 2023) and clumped isotope thermometry (Xu et al., 2023) also suggest the rise of Gangdese mountains prior to the India-Eurasia collision, which may have been an isostatic compensation response to crust thickening during the Late Cretaceous.

5.2. Estimating S oxidation state in the melt from apatite S content

Minimum $S^{6+}/\Sigma S$ in the melt can be estimated from S content in apatite. We followed the approaches of Tang et al. (2020) and Wang et al. (2025a) and calculated S^{2-} and S^{6+} partitioning between apatite and melt separately. For S^{2-}, we used SCSS under reduced conditions as the maximum S^{2-} concentration in the melt. Because S^{2-} is incompatible in apatite, we assumed $D_{S^{2-}}^{ap/m} = 1$ as an upper bound. These assumptions allow us to calculate the maximum S^{2-} in apatite, and any excess S in apatite must be S^{6+}. We then used this excess S (as S^{6+}) to calculate S^{6+} concentration in the melt based on the empirical partitioning equation from Parat et al. (2011). With this calculated S^{6+} concentration and the maximum S^{2-} concentration in the melt (= SCSS under reduced conditions), the minimum $S^{6+}/\Sigma S$ in the melt can be derived (the detailed calculation procedures are provided in the Supplementary Material).

The calculation described above critically relies on the contrasting partitioning behaviors of S^{6+} and S^{2-} between apatite and melt. The incompatibility of S^{2-} in apatite is supported by a number of

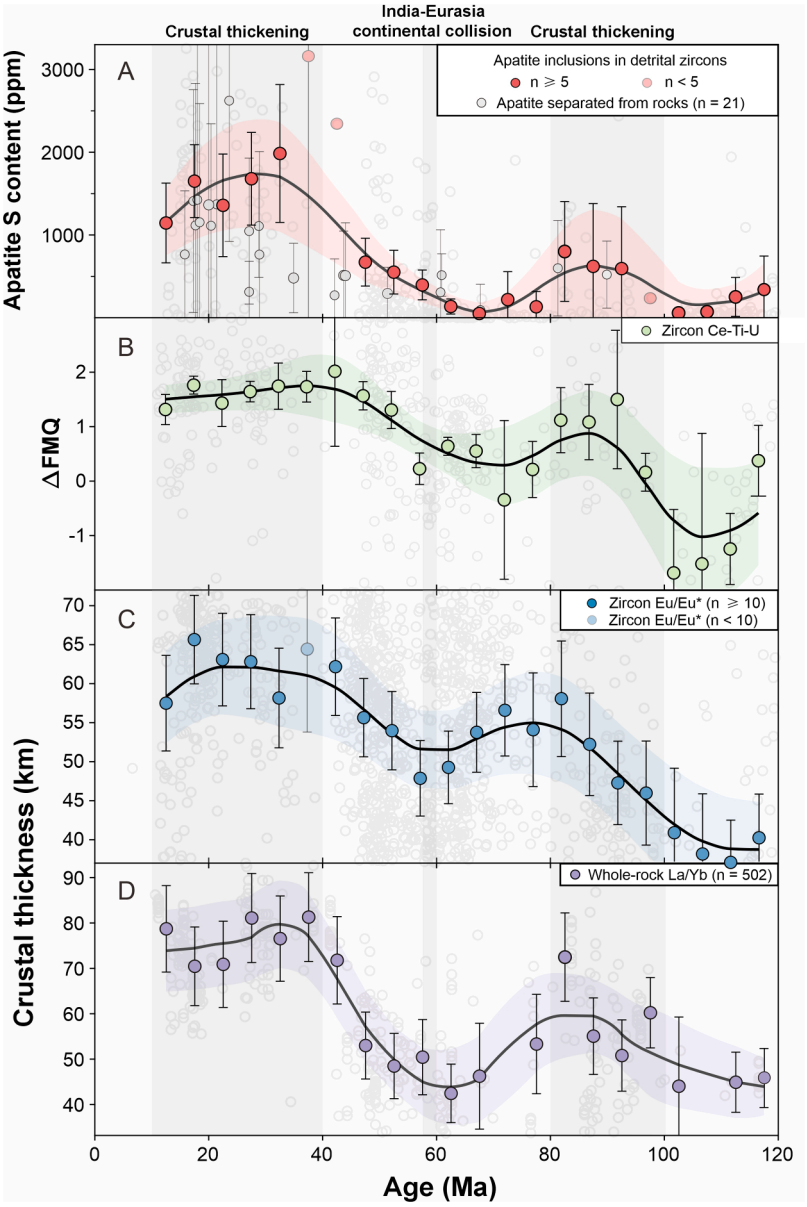


Fig. 2. Evolution of magmatic oxidation state and crustal thickness in the eastern Gangdese. All data are plotted as binned averages (bin size = 5 Myr) and 2 SE. A smoothed trend with 95% confidence intervals is shown in each subplot as a black curve with shaded envelopes. (A) S content in apatite inclusions hosted in detrital zircons. The data of apatite separated from rocks are from Tang et al. (2020). (B) Evolution of oxygen fugacity of Gangdese felsic magmas calculated using the zircon Ce-U-Ti oxybarometer. (C) Crustal thickness reconstructed using detrital zircon Eu/Eu*. (D) Crustal thickness estimated from whole-rock La/Yb ratio of intermediate and felsic rocks (SiO2 contents of 55-70 wt%). The two grey vertical bands on either side represent periods of crustal thickening. The middle gray vertical line marks the timing of India-Eurasia collision (Hu et al., 2017). The results using a wider bin size of 10 Myr are shown in the Supplementary Material (Fig. S9).

experimental studies. For example, Peng et al. (1997) reported that under relatively reduced conditions (at FMQ), where sulfur in silicate melts occurs predominantly as S^{2-}, apatite crystallized from S-saturated silicate melts contains sulfur below the detection limit. A more recent study by Konecke et al. (2019) directly quantified S speciation in apatite and demonstrated that $D_S^{ap/m}$ are 0.02 (±0.01) at ΔFMQ = -1 and 0.13 (±0.02) at FMQ, both significantly lower than 1. For S^{6+} partitioning between apatite and melt, we adopted empirical equation reported by Parat et al. (2011) to represent the behavior S^{6+} of between apatite and melt, as the experimental dataset used for their parameterization was obtained at high fO_2 conditions, where S in the melt is predominantly present as S^{6+}.

There are several simplifications in our calculation that warrant additional explanation. The partitioning behavior of S^{6+} between apatite and melt is pressure-independent but temperature-dependent (Peng et al., 1997). We are unable to quantify the effect of temperature on S^{6+} partitioning in our model, but this influence is limited and secondary to that of fO_2 on S partitioning. Using Ti-in-zircon thermometer (Ferry and Watson, 2007), we calculated the temperatures of Gangdese felsic magmas. The results show that the average temperature of the system does not change significantly with age (Fig. S14) and does not covary with apatite S content (Fig. 3A). Variations in P-T and S content in the melt, and redox heterogeneity in the magma chamber due to recharge/assimilation may account for the fluctuations in S content of individual apatite grains.

Our calculated $S^{6+}/\Sigma S$ correlates with the fO_2 derived from zircon Ce-U-Ti oxybarometer (Fig. 3B), in contrast to its lack of correlation with temperature. In particular, the sharp increase in $S^{6+}/\Sigma S$ under oxidized conditions matches theoretical predictions if the zircon and apatite crystallized at 600-800 °C, which is consistent with the Ti-in-zircon

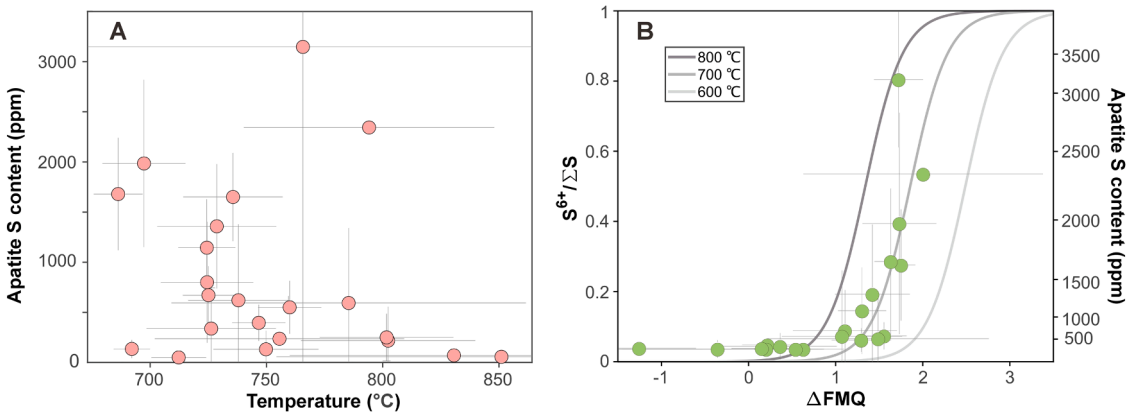


Fig. 3. (A) Average apatite S content vs. magma temperature of each age bin defined in Fig. 2. The temperature was calculated by Ti-in-zircon thermometer (Ferry and Watson, 2007), assuming $\alpha_{SiO_2} = 1$ and $\alpha_{TiO_2} = 0.8$. Error bars represent ±2 SE. (B) Calculated minimum magmatic $S^{6+}/\Sigma S$ vs. ΔFMQ of the magma. The relationship between magmatic $S^{6+}/\Sigma S$ and S contents in apatite is calculated based on the method described in Supplementary Materials. The three grey curves show the model-predicted $S^{6+}/\Sigma S$ ratios (left axis) as a function of ΔFMQ at temperatures and a composition typical of felsic magmas Sun and Yao, (2024). Error bars represent ±2 SE.

temperatures (Fig. S14). These results reinforce our key assumption that high S contents in apatite inclusions are indicative of sulfate-bearing oxidized melts and apatite S content can be used to approximate $S^{6+}/\Sigma S$ in the melt.

5.3. *Relationships between crustal thickening, S oxidation, and magma fO_2*

Our results show two episodes of significantly elevated apatite S contents in the eastern Gangdese over the past 120 Myr: one during 95-80 Ma, and another during 45-10 Ma. The younger episode of S oxidation is consistent with the data of apatite grains separated from rock samples reported by Tang et al. (2020) (Fig. 2A). However, the Late Cretaceous episode was not identified by Tang et al. (2020), likely due to their limited number of samples (n = 2) from that period. Nevertheless, the two Cretaceous samples in Tang et al. (2020) have similar average apatite S contents to those of our apatite inclusions in detrital zircons (Fig. 2A). These results demonstrate the advantage of using apatite inclusions in detrital zircons to reconstruct S oxidation history on orogen scales.

The magma fO_2 calculated from zircon Ce-U-Ti oxybarometer (Fig. 2B) follows a similar trend to that of apatite S content (Fig. 2A).

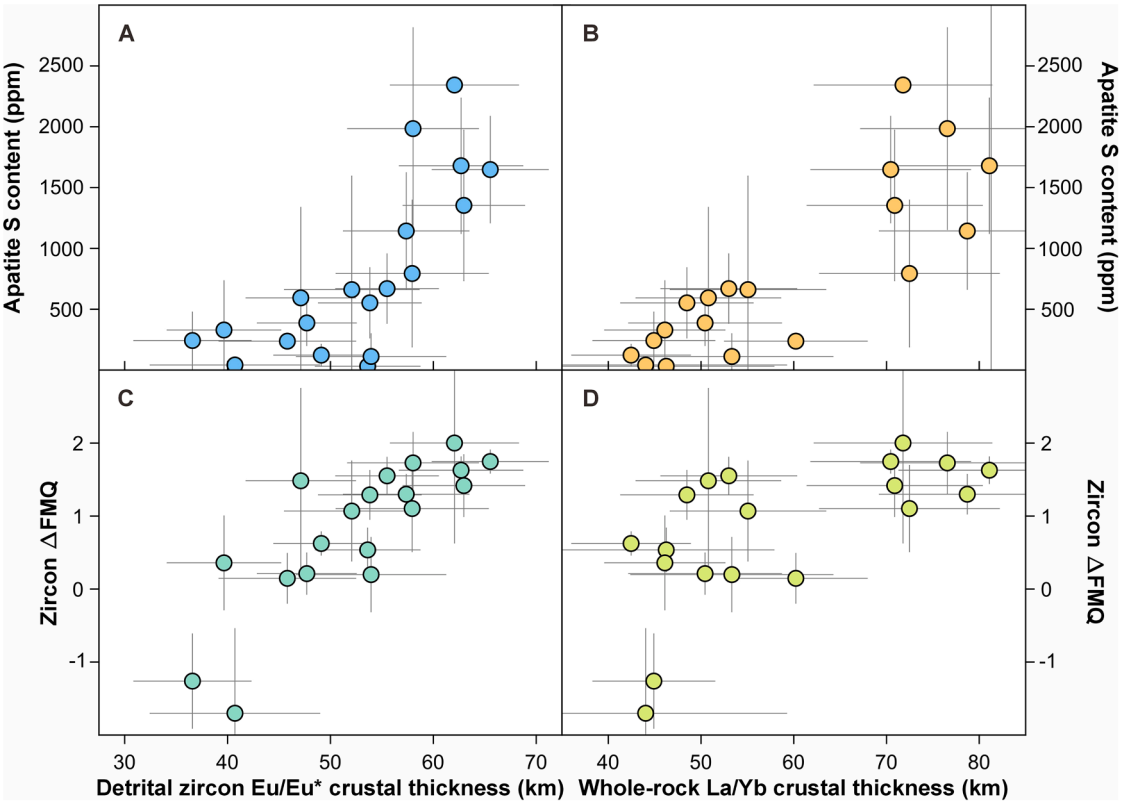


Fig. 4. Plot of average apatite S and magma fO_2 versus average crustal thickness of each age bin defined in Fig. 2. The crustal thickness was calculated from detrital zircon Eu/Eu* (A, C) and whole-rock La/Yb (B, D). Error bars represent ±2 SE.

This consistency is not surprising because sulfate is compatible in apatite whereas sulfide is not as discussed above. Critically, the timing of magmatic S oxidation (high apatite S contents) and elevated magma fO_2 aligns precisely with the two episodes of crustal thickening in the eastern Gangdese (Fig. 2C and 2D). The reduction in S content in apatite and magma fO_2 also temporally coincides with crustal thinning during 120-100 Ma and 80-60 Ma. By plotting apatite S content, fO_2 and crustal thickness directly, Fig. 4 confirms the strong positive correlations between the extent of S oxidation, magma fO_2, and crustal thickness.

The coevolution between magmatic S oxidation state, magma fO_2, and crustal thickness is consistent with differentiation-dependent magma oxidation, and this oxidation is pressure-controlled. Given that Fe^{3+}-Fe^{2+} is the primary redox pair in silicate melts, magmatic fO_2 and $S^{6+}/\Sigma S$ are highly depended on the $Fe^{3+}/\Sigma Fe$ ratio. Consequently, any magmatic differentiation process that alters the Fe^{3+}/Fe^{2+} ratio in the melt may influence the oxidation state of the magma. The fractional crystallization of principal Fe-bearing minerals (e.g. amphibole, magnetite, and garnet) exerts a significant control on the $Fe^{3+}/\Sigma Fe$ ratio of the residual melt. Globally, arc magmas in continental arcs with thick crust commonly exhibit an Fe-depleting trend with differentiation (Chen et al., 2023). While magnetite crystallization can decrease the Fe content of the melt, it cannot increase the $Fe^{3+}/\Sigma Fe$ ratio because magnetite contains a high proportion of Fe^{3+}. In addition, at high pressures in thickened crust, magnetite saturation is suppressed, preventing it from becoming a major crystallizing phase (Blatter et al., 2013; Tang et al., 2023).

Garnet, on the contrary, stabilizes as a fractionating/residual phase under high pressures. This is supported by a series of experimental results summarized by Chen et al. (2023), which indicate that garnet becomes stable at ~1.0 GPa at 1000 °C and at ~1.5 GPa at 1150 °C in hydrous basaltic systems. Recent studies on Fe isotopes and MREE/HREE fractionations of global magmas exhibiting strong calc-alkaline characteristics have highlighted the role of garnet as an important phase responsible for Fe depletion in these evolved arc magmas (Chen et al., 2023; Du et al., 2022; Li et al., 2021; Liang et al., 2022). Garnet preferentially removes Fe^{2+} from the melt, which can raise the $Fe^{3+}/\Sigma Fe$ ratio of the residual melt and cause magmatic oxidation (Tang et al., 2018; Tang et al., 2019). This mechanism was initially proposed based on the Eu systematics in arclogites (Tang et al., 2018). Subsequent Fe valence analyses confirmed the low $Fe^{3+}/\Sigma Fe$ (0.04-0.08) in garnet from these deep arc cumulates (Tang et al., 2019). Although Holycross and Cottrell (2023) questioned the oxidative capacity of garnet, subsequent corrections to their models show that garnet-dominated fractionation can significantly raise magmatic fO_2 (Tang et al., 2024b). We thus suggest that garnet fractionation during crustal thickening provides a viable explanation for the observed coevolution between magmatic S oxidation state, magma fO_2, and crustal thickness in the eastern Gangdese.

The role of garnet fractionation in Gangdese magmatism has also been highlighted by several recent studies. For example, whole-rock Dy/Yb ratios (a sensitive tracer of garnet fractionation) of granitic rock from the eastern Gangdese significantly increased with intense crustal thickening after India-Eurasia collision (Tang et al., 2020). Similar results have also been reported for ~43 Ma granites in the western Gangdese (Wang et al., 2015a). A more recent study found that a juvenile and continuous continental lower-crustal section in the Gangdese Arc (formed during the crustal thickening episode in Late Cretaceous) shows relatively light Ca isotopic compositions, interpreted to reflect crystallization/segregation of garnet-bearing (~20%) cumulates (Wang et al., 2025b). Common conversion point imaging across the Gangdese batholith also reveals a widely distributed lower-crustal doublet at depths of 60-80 km (Xu et al., 2015), which is seismically interpreted to represent an eclogite (garnet-rich) layer (Wittlinger et al., 2009). These findings collectively suggest that garnet fractionation/retention is widespread in the lower crust of the Gangdese. According to the lower-crustal partial melting model established by Tang et al. (2020), such a proportion of residual garnet (~20%) in a basaltic lower crust (FeO_T = 8.5 wt.%, $Fe^{3+}/\Sigma Fe$ = 0.16; melt fraction (F) = 30%) is sufficient to shift the dominant S species from S^{2-} to S^{6+} in the derived melt.

Amphibole fractionation has also been proposed to increase the $Fe^{3+}/\Sigma Fe$ ratio in residual melts (Luo et al., 2024; Zhang et al., 2022), although the partition coefficient ratio D_{Fe3+}/D_{Fe2+} between amphibole and melt is close to or even greater than 1 (Goltz et al., 2022). The high D_{Fe3+}/D_{Fe2+} may limit the efficiency of amphibole fractionation in removing Fe^{2+} from the melt. For example, Luo et al. (2024) studied a suite of Miocene samples in the Gangdese and found that extensive amphibole fractionation caused only ~0.8 log units increase in fO_2. The role of amphibole may require additional experiments on Fe partitioning.

Another proposed mechanism is that water induces oxidation of magmas if it degasses as H_2 (Humphreys et al., 2015; Sato and Wright, 1966). This mechanism is also appealing because in arcs with thick crusts, differentiation may lead to more hydrous evolved magmas than those in arcs with thin crusts (Klein et al., 2023; Nathwani et al., 2024), which may enhance water induced oxidation. However, there are also a number of studies showing that the redox state of the magmas appears to be decoupled from their water contents (e.g., Gaillard et al. (2003); Portnyagin et al. (2012); Waters and Lange (2016)). These studies questioned the efficiency of magma oxidation by water break down and H_2 loss. More work on how magma fO_2 evolves during water degassing/fluid exsolution is needed to further test the role of water in oxidizing crustal magmas.

To summarize, our observations of coupled evolution of S redox state, magmatic fO_2, and crustal thickness, together with recent studies on magmatic differentiation at thickened arcs, led us to conclude that garnet (± amphibole) fractionation/retention was critical in driving the oxidation of felsic magmas in the Gangdese.

5.4. The influence of source composition on the oxidation of Gangdese felsic magmas

Oxidation of arc magmas may also take place in the mantle wedge via incorporation of oxidized aqueous fluids or sediment melts derived from the descending slabs (Cottrell et al., 2025; Evans, 2012). There is no doubt that observations supporting arc mantle oxidation are abundant (Brounce et al., 2014; Evans et al., 2012; Kelley and Cottrell, 2009; Nathwani et al., 2025). But the nature of the slab components (oxidized or reduced) appears complicated (Li et al., 2020; Piccoli et al., 2019) and there are different opinions as to the extent to which the complex slab components alter the redox state of arc magmas (Lee et al., 2012; Lee et al., 2010; Li and Lee, 2004; Mallmann and O'Neill, 2009). To the problem of interest here, a further complication is whether the oxidation signatures of primitive arc magmas can be effectively transmitted to felsic magmas after extensive intracrustal differentiation.

To evaluate whether the temporal variation in S oxidation in the Gangdese felsic magmas reflects redox signatures of their mafic precursors, we examined the V/Sc ratio, a widely used indicator of the redox state of primitive magmas (Li and Lee, 2004), in mafic rocks from the Gangdese. Data for mafic rocks are from Tibetan magmatism database (Chapman and Kapp, 2017) and listed in Supplementary Data 1. We emphasize that V/Sc serves as a reliable proxy of mantle fO_2 only in primitive samples with MgO > 8 wt.%, where magma differentiation is dominated by olivine fractionation and thus exerts minimal influence on melt V/Sc (Canil, 2004; Lee et al., 2005; Li and Lee, 2004). This assumption is supported by the absence of systematic variation in V/Sc with decreasing MgO at MgO > 8 wt.% in our data (Fig. S8). In the Gangdese, primitive mafic samples with 8-12 wt.% MgO show average V/Sc ratios of 6-7 (Fig. 5), corresponding to ΔFMQ values of -0.5 to +1, depending on the calibration models used (Lee et al., 2005; Wang et al., 2019). These mildly oxidized conditions can barely oxidize S in felsic magmas (Fig. 3B). More importantly, the average V/Sc ratios of these mafic samples show no significant temporal variation, whereas the

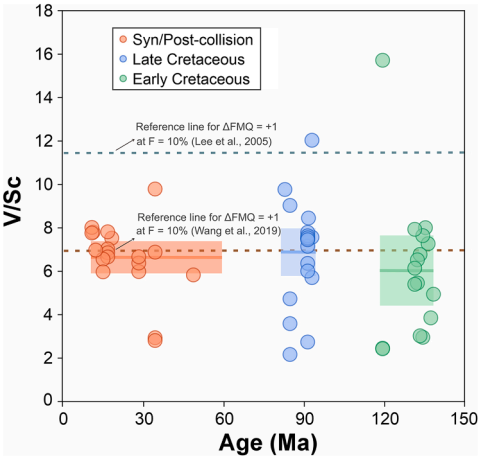


Fig. 5. V/Sc ratios of mafic rock through time. Solid horizontal lines with different colors are averages over the given time period: 6.0 ± 1.6 (2SE) for Early Cretaceous, 6.9 ± 1.1 (2SE) for Late Cretaceous, 6.6 ± 0.7 (2SE) for syn/post-collision stage. For comparison, the two dashed lines show the V/Sc ratios of primary magmas at F = 10% and ΔFMQ = +1 modeled by Lee et al. (2005) and Wang et al. (2019).

oxidation states of felsic magmas vary significantly through time (Fig. 2). This decoupling contrasts with the coupling between felsic magma oxidation and crustal thickness, and suggests that the redox state of mafic parental magmas/rocks as well as the mantle sources may have had limited influences on the redox state of Gangdese felsic magmas.

5.5. *Implications for the genesis and exploration of porphyry Cu systems*

Our results imply that crustal thickening-induced garnet (± amphibole) fractionation/retention plays a key role in driving S oxidation in magmatic orogens. Meanwhile, the influence of slab-derived components on the redox state of felsic magmas appears to be limited, which may be explained if the redox signatures of primary arc magmas/protoliths are largely overprinted during intracrustal differentiation. This is consistent with the modeling study of Sun and Lee (2022). Assimilation of deep buried sediments in arc crust may also have an impact on the redox of differentiated magmas. This process may explain the occasional high apatite S contents in individual apatite inclusions during 60-50 Ma when the crust was relatively thin (Fig. 2A). But still, the average apatite S contents within this time period are significantly lower than those during intense crustal thickening.

Endogenic oxidation may provide a universal mechanism linking the redox state of felsic magmas to tectonics. As the crust thickens, S in the felsic magmas becomes progressively oxidized, suppressing extensive sulfide saturation during fractional crystallization and second boiling in upper crustal magma reservoirs (Jugo, 2009). This process prevents extensive Cu sequestration by sulfides and facilitates Cu complexation in ore-forming fluids (Richards, 2015).

Our results highlight measuring S content in detrital zircon-hosted apatite inclusions as a robust and efficient approach to probe S oxidation in felsic magmas on orogen scales. Provenance analysis of river sands enables direct linkage between detrital zircon grains to their upstream magmatic sources. When combined with measurements of apatite inclusions, this approach offers a novel and convenient means for assessing magmatic S redox evolution and porphyry Cu fertility across specific regions in orogenic belts. As Fig. 6 shows, river sands draining known large to giant porphyry Cu districts yield zircon-hosted apatite inclusions with a distinctly higher proportion of S-rich (> 1000 ppm) inclusions. This observation validates the effectiveness of this new method. Additionally, one locality (sample XY-6), despite the absence of known PCDs, exhibits elevated S-rich apatite signatures, suggesting considerable potential for undiscovered mineralization.

While elevated average apatite S contents are related to PCD formation, the absence of Late Cretaceous PCDs raises questions. Nevertheless, it should be noted that in the Late Cretaceous, the Gangdese Belt underwent intense deformation and rapid uplift, which coincides with a regional angular unconformity and significant crustal exhumation of the Gangdese batholith (Cao et al., 2020; Ma et al., 2023; Xu et al., 2023). We infer that even if PCDs did form at this time, they may not be preserved owing to tectonics-driven exhumation and erosion of these shallow-level intrusions at 2-5 km depths.

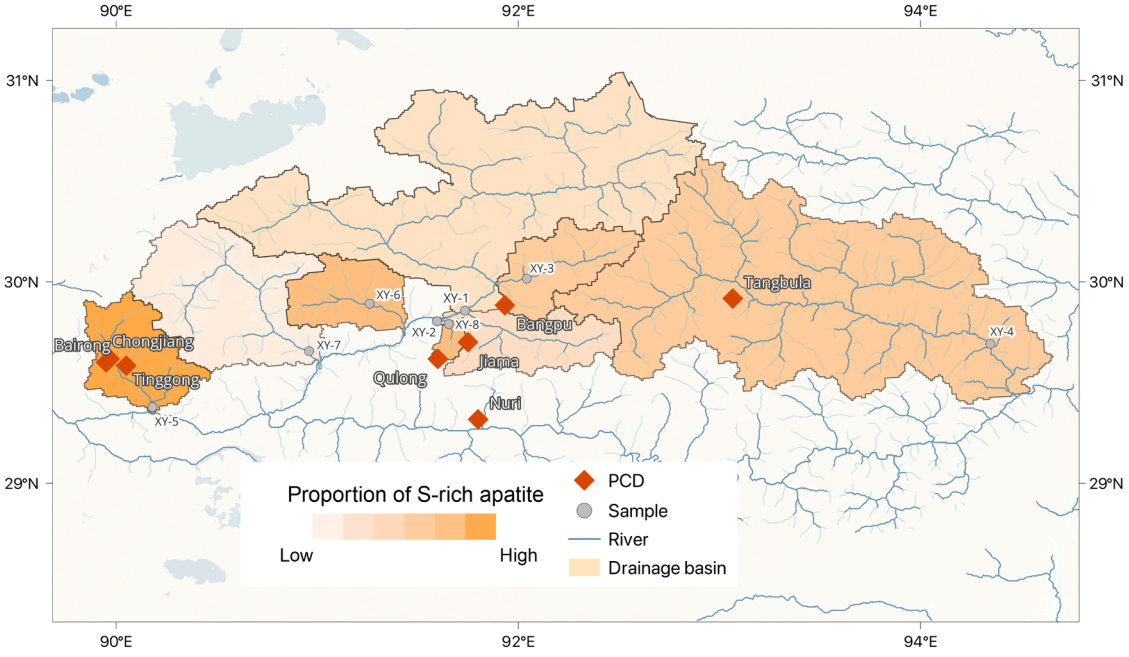


Fig. 6. Map showing proportions of S-rich zircon-hosted apatite inclusions in each river sand sample and their corresponding drainage areas.

6. Conclusions

We measured S content of apatite inclusions within detrital zircons to reconstruct the magmatic S redox evolution across the eastern Gangdese. This new approach allows us to capture major episodes of S oxidation in felsic magmas on orogen scales and evaluate the temporal correlation between S oxidation and crustal thickening. Below, we summarize our major findings.

1. In the eastern Gangdese, apatite S contents rose during the Late Cretaceous and from the Late Paleocene to the Miocene, and both high apatite S episodes were accompanied by crustal thickening.
2. The coevolution between apatite S content, magma fO_2 and crustal thickness is most likely an outcome of garnet (± amphibole) fractionation/retention in the deep crust, which is modulated by the differentiation pressure/crustal thickness. On the contrary, the influence of source composition on the oxidation of felsic magmas may be limited.
3. Crustal thickening-induced endogenic oxidation may play a critical role in driving S oxidation of felsic magmas and promoting the generation of porphyry Cu deposits.
4. Measurements of apatite inclusions in detrital zircons, combined with provenance analysis, may provide an effective and convenient approach for probing S oxidation in felsic magmas on orogen scales and evaluating regional porphyry-Cu mineralization potential.

CRediT authorship contribution statement

Xuyang Zheng: Data curation, Formal analysis, Investigation, Methodology, Visualization, Writing – original draft. **Ming Tang:** Conceptualization, Funding acquisition, Investigation, Writing – review & editing. **Hao Chen:** Investigation, Visualization, Writing – review & editing. **Ziyi Guo:** Investigation, Visualization.

Declaration of competing interest

The authors declare that they have no known competing financial interests or personal relationships that could have appeared to influence the work reported in this paper.

Acknowledgements

We thank Chetan Nathwani and one anonymous reviewer for their constructive comments. We thank Jiazhen Wang for his assistance during the EPMA analysis and Hongyan Fan for her help during the LA-ICP-MS analysis. We also thank our colleagues Xi Huang, Runwu Li, Junteng Lyu, Jiazhen Wang and Zi Ye for their assistance during sample collection. This work was financially supported by National Natural Science Foundation of China (grants 42488201 and 42125302). M. Tang is grateful for the support from the New Cornerstone Science Foundation through the XPLORER PRIZE.

Supplementary materials

Supplementary material associated with this article can be found, in the online version, at doi:10.1016/j.epsl.2026.120220.

Data availability

The data used in this paper are included in the Supplemental Data 1.

References

Allegre, C.o., Courtillot, V., Tapponnier, P., Hirn, A., Mattauer, M., Coulon, C., Jaeger, J., Achache, J., Schärer, U., Marcoux, J., 1984. Structure and evolution of the Himalaya–Tibet orogenic belt. Nature 307, 17–22.

Annen, C., Blundy, J., Sparks, R., 2006. The genesis of intermediate and silicic magmas in deep crustal hot zones. Journal of petrology 47, 505–539.

Audétat, A., Chang, J., Gaynor, S.P., 2025a. Widespread anhydrite saturation in Laramide-age arc magmas of the southwestern USA. Geology.

Audétat, A., Chang, J., Gaynor, S.P., 2025b. Widespread Occurrence of Former Anhydrite Phenocrysts in Laramide-Age Magmas Related to Porphyry–Skarn Cu Mineralization at Santa Rita and Hanover-Fierro. Journal of Petrology 66, egaf002.

Beaudry, P., Sverjensky, D.A., 2024. Oxidized sulfur species in slab fluids as a source of enriched sulfur isotope signatures in arcs. Geochemistry, Geophysics, Geosystems 25, e2024GC011542.

Blatter, D.L., Sisson, T.W., Hankins, W.B., 2013. Crystallization of oxidized, moderately hydrous arc basalt at mid-to lower-crustal pressures: implications for andesite genesis. Contributions to Mineralogy and Petrology 166, 861–886.

Brounce, M.N., Kelley, K.A., Cottrell, E., 2014. Variations in Fe3+/∑Fe of Mariana Arc Basalts and Mantle Wedge fO2. Journal of Petrology 55, 2513–2536.

Canil, D., 2004. Mildly incompatible elements in peridotites and the origins of mantle lithosphere. Lithos 77, 375–393.

Cao, W., Yang, J., Zuza, A.V., Ji, W.-Q., Ma, X.-X., Chu, X., Burgess, Q.P., 2020. Crustal tilting and differential exhumation of Gangdese Batholith in southern Tibet revealed by bedrock pressures. Earth and Planetary Science Letters 543, 116347.

Chambefort, I., Dilles, J.H., Kent, A.J., 2008. Anhydrite-bearing andesite and dacite as a source for sulfur in magmatic-hydrothermal mineral deposits. Geology 36, 719–722.

Chang, J., Li, J.-W., Audétat, A., 2018. Formation and evolution of multistage magmatic-hydrothermal fluids at the Yulong porphyry Cu-Mo deposit, eastern Tibet: Insights from LA-ICP-MS analysis of fluid inclusions. Geochimica et Cosmochimica Acta 232, 181–205.

Chapman, J.B., Kapp, P., 2017. Tibetan magmatism database. Geochemistry, Geophysics, Geosystems 18, 4229–4234.

Chen, K., Tang, M., Hu, Z., Liu, Y., 2023. Generation of tholeiitic and calc-alkaline arc magmas and its implications for continental growth. Geochimica et Cosmochimica Acta 355, 173–183.

Cottrell, E., Canil, D., Langmuir, C., Evans, K.A., Gaillard, F., 2025. Earth's past and present mantle oxygen fugacity. Nature Reviews Earth & Environment 6, 728–746.

Du, D.-H., Tang, M., Li, W., Kay, S.M., Wang, X.-L., 2022. What drives Fe depletion in calc-alkaline magma differentiation: Insights from Fe isotopes. Geology 50, 552–556.

Evans, K.A., 2012. The redox budget of subduction zones. Earth-Science Reviews 113, 11–32.

Evans, K.A., Elburg, M.A., Kamenetsky, V.S., 2012. Oxidation state of subarc mantle. Geology 40, 783–786.

Ferry, J., Watson, E., 2007. New thermodynamic models and revised calibrations for the Ti-in-zircon and Zr-in-rutile thermometers. Contributions to Mineralogy and Petrology 154, 429–437.

Gaillard, F., Pichavant, M., Scaillet, B., 2003. Experimental determination of activities of FeO and Fe2O3 components in hydrous silicic melts under oxidizing conditions. Geochimica et Cosmochimica Acta 67, 4389–4409.

Goltz, A.E., Krawczynski, M.J., McCanta, M.C., Darby Dyar, M., 2022. Experimental calibration of an Fe3+/Fe2+-in-amphibole oxybarometer and its application to shallow magmatic processes at Shiveluch Volcano, Kamchatka. American Mineralogist 107, 2084–2100.

Grondahl, C., Zajacz, Z., 2022. Sulfur and chlorine budgets control the ore fertility of arc magmas. Nat Commun 13, 4218.

Holycross, M., Cottrell, E., 2023. Garnet crystallization does not drive oxidation at arcs. Science 380, 506–509.

Hou, Z., Duan, L., Lu, Y., Zheng, Y., Zhu, D., Yang, Z., Yang, Z., Wang, B., Pei, Y., Zhao, Z., 2015. Lithospheric architecture of the Lhasa terrane and its control on ore deposits in the Himalayan-Tibetan orogen. Economic Geology 110, 1541–1575.

Hu, X., Wang, J., An, W., Garzanti, E., Li, J., 2017. Constraining the timing of the India-Asia continental collision by the sedimentary record. Science China Earth Sciences 60, 603–625.

Huang, F., Zhou, C., Wang, W., Kang, J., Wu, Z., 2019. First-principles calculations of equilibrium Ca isotope fractionation: Implications for oldhamite formation and evolution of lunar magma ocean. Earth and Planetary Science Letters 510, 153–160.

Humphreys, M.C.S., Brooker, R.A., Fraser, D.G., Burgisser, A., Mangan, M.T., McCammon, C., 2015. Coupled Interactions between Volatile Activity and Fe Oxidation State during Arc Crustal Processes. Journal of Petrology 56, 795–814.

Hutchinson, M.C., Dilles, J.H., 2019. Evidence for magmatic anhydrite in porphyry copper intrusions. Economic Geology 114, 143–152.

Ibarra, D.E., Dai, J., Gao, Y., Lang, X., Duan, P., Gao, Z., Chen, J., Methner, K., Sha, L., Tong, H., Han, X., Zhu, D., Li, Y., Tang, J., Cheng, H., Chamberlain, C.P., Wang, C., 2023. High-elevation Tibetan Plateau before India–Eurasia collision recorded by triple oxygen isotopes. Nature Geoscience 16, 810–815.

Ji, W.-Q., Wu, F.-Y., Chung, S.-L., Li, J.-X., Liu, C.-Z., 2009. Zircon U–Pb geochronology and Hf isotopic constraints on petrogenesis of the Gangdese batholith, southern Tibet. Chemical Geology 262, 229–245.

Ji, W.-Q., Wu, F.-Y., Chung, S.-L., Liu, C.-Z., 2014. The Gangdese magmatic constraints on a latest Cretaceous lithospheric delamination of the Lhasa terrane, southern Tibet. Lithos 210, 168–180.

Jugo, P.J., 2009. Sulfur content at sulfide saturation in oxidized magmas. Geology 37, 415–418.

Kelley, K.A., Cottrell, E., 2009. Water and the oxidation state of subduction zone magmas. Science 325, 605–607.

Klein, B.Z., Jagoutz, O., Schmidt, M.W., Kueter, N., 2023. A global assessment of the controls on the fractionation of arc magmas. Geochemistry, Geophysics, Geosystems 24, e2023GC010888.

Konecke, B.A., Fiege, A., Simon, A.C., Linsler, S., Holtz, F., 2019. An experimental calibration of a sulfur-in-apatite oxybarometer for mafic systems. Geochimica et Cosmochimica Acta 265, 242–258.
Konecke, B.A., Fiege, A., Simon, A.C., Parat, F., Stechern, A., 2017. Co-variability of S6+, S4+, and S2−in apatite as a function of oxidation state: Implications for a new oxybarometer. American Mineralogist 102, 548–557.
Lee, C.-T., Leeman, W.P., Canil, D., Li, Z.-X.A., 2005. Similar V/Sc Systematics in MORB and Arc Basalts: Implications for the Oxygen Fugacities of their Mantle Source Regions. Journal of Petrology 46, 2313–2336.
Lee, C.-T.A., Luffi, P., Chin, E.J., Bouchet, R., Dasgupta, R., Morton, D.M., Le Roux, V., Yin, Q.-z., Jin, D., 2012. Copper systematics in arc magmas and implications for crust-mantle differentiation. Science 336, 64–68.
Lee, C.T., Luffi, P., Le Roux, V., Dasgupta, R., Albarede, F., Leeman, W.P., 2010. The redox state of arc mantle using Zn/Fe systematics. Nature 468, 681–685.
Lee, C.-T.A., Tang, M., 2020. How to make porphyry copper deposits. Earth and Planetary Science Letters 529.
Leier, A.L., DeCelles, P.G., Kapp, P., Gehrels, G.E., 2007. Lower Cretaceous strata in the Lhasa Terrane, Tibet, with implications for understanding the early tectonic history of the Tibetan Plateau. Journal of Sedimentary Research 77, 809–825.
Li, J.-L., Schwarzenbach, E.M., John, T., Ague, J.J., Huang, F., Gao, J., Klemd, R., Whitehouse, M.J., Wang, X.-S., 2020. Uncovering and quantifying the subduction zone sulfur cycle from the slab perspective. Nature Communications 11.
Li, Q.W., Nebel-Jacobsen, Y., Zhao, J.H., Nebel, O., Richter, M., Cawood, P.A., Wang, Q., 2021. An Early Garnet Redox-Filter as an Additive Oxidizer in Lower Continental Arc Crust Traced Through Fe Isotopes. Journal of Geophysical Research: Solid Earth 126, e2020JB021217.
Li, Z.-X., Lee, C.-T., 2004. The constancy of upper mantle fO2 through time inferred from V/Sc ratios in basalts. Earth and Planetary Science Letters 228, 483–493.
Liang, W., Huang, J., Zhang, G., Huang, F., 2022. Iron isotopic fractionation during eclogite anatexis and adakitic melt evolution: insights into garnet effect on Fe isotopic variations in high-silica igneous rocks. Contributions to Mineralogy and Petrology 177, 33.
Loucks, R.R., Fiorentini, M.L., Henríquez, G.J., 2020. New Magmatic Oxybarometer Using Trace Elements in Zircon. Journal of Petrology 61.
Loucks, R.R., Henríquez, G.J., Fiorentini, M.L., 2024. Zircon and whole-rock trace element indicators of magmatic hydration state and oxidation state discriminate copper ore-forming from barren arc magmas. Economic Geology 119, 511–523.
Luo, C.-H., Wang, R., Nebel, O., Li, Q.-W., 2024. Amphibole fractionation as a key driver for oxidation of magmas in convergent margins. Earth and Planetary Science Letters 641.
Ma, X., Xu, Z., Lusk, A.D., Erdmann, S., Chen, X., Ma, S., 2023. Late Cretaceous tectonothermal events of the Gangdese belt, southern. Tibet. Geosphere 19, 933–956.
Mallmann, G., O'Neill, H.S.C., 2009. The Crystal/Melt Partitioning of V during Mantle Melting as a Function of Oxygen Fugacity Compared with some other Elements (Al, P, Ca, Sc, Ti, Cr, Fe, Ga, Y, Zr and Nb). Journal of Petrology 50, 1765–1794.
Meng, X., Simon, A.C., Kleinsasser, J.M., Mole, D.R., Kontak, D.J., Jugo, P.J., Mao, J., Richards, J.P., 2022. Formation of oxidized sulfur-rich magmas in Neoarchaean subduction zones. Nature Geoscience 15, 1064–1070.
Muth, M.J., Wallace, P.J., 2022. Sulfur recycling in subduction zones and the oxygen fugacity of mafic arc magmas. Earth and Planetary Science Letters 599.
Nathwani, C., Blundy, J., Large, S.J.E., Wilkinson, J.J., Buret, Y., Loader, M.A., Tavazzani, L., Chelle-Michou, C., 2024. A zircon case for super-wet arc magmas. Nature Communications 15.
Nathwani, C., Giovanini, E., Bachmann, O., Sossi, P., Allaz, J., Cotte, M., Candioti, L., Chelle-Michou, C., 2025. Sulfate-dominant apatite in the deep arc crust indicates that high oxidation state promotes copper fluxing in arcs. Geology 54, 87–91.
Nathwani, C.L., Large, S.J.E., Brugge, E.R., Wilkinson, J.J., Buret, Y., 2023. Apatite evidence for a fluid-saturated, crystal-rich magma reservoir forming the Quellaveco porphyry copper deposit (Southern Peru). Contributions to Mineralogy and Petrology 178.
Parat, F., Holtz, F., Streck, M.J., 2011. Sulfur-bearing magmatic accessory minerals. Reviews in Mineralogy and Geochemistry 73, 285–314.
Park, J.-W., Campbell, I.H., Chiaradia, M., Hao, H., Lee, C.-T., 2021. Crustal magmatic controls on the formation of porphyry copper deposits. Nature Reviews Earth & Environment 2, 542–557.
Peng, G., Luhr, J.F., McGee, J.J., 1997. Factors controlling sulfur concentrations in volcanic apatite. American Mineralogist 82, 1210–1224.
Piccoli, F., Hermann, J., Pettke, T., Connolly, J., Kempf, E.D., Vieira Duarte, J., 2019. Subducting serpentinites release reduced, not oxidized, aqueous fluids. Scientific Reports 9, 19573.
Portnyagin, M., Hoernle, K., Storm, S., Mironov, N., van den Bogaard, C., Botcharnikov, R., 2012. H2O-rich melt inclusions in fayalitic olivine from Hekla volcano: implications for phase relationships in silicic systems and driving forces of explosive volcanism on Iceland. Earth and Planetary Science Letters 357, 337–346.
Profeta, L., Ducea, M.N., Chapman, J.B., Paterson, S.R., Gonzales, S.M.H., Kirsch, M., Petrescu, L., DeCelles, P.G., 2015. Quantifying crustal thickness over time in magmatic arcs. Scientific Reports 5.
Richards, J.P., 2015. The oxidation state, and sulfur and Cu contents of arc magmas: implications for metallogeny. Lithos 233, 27–45.
Richards, J.P., 2021. Porphyry copper deposit formation in arcs: What are the odds? Geosphere 18, 130–155.
Sato, M., Wright, T.L., 1966. Oxygen fugacities directly measured in magmatic gases. Science 153, 1103–1105.
Sillitoe, R.H., 2010. Porphyry Copper Systems. Economic Geology 105, 3–41.
Stormer, J.C., Pierson, M.L., Tacker, R.C., 1993. Variation of F and Cl X-ray intensity due to anisotropic diffusion in apatite during electron microprobe analysis. American Mineralogist 78, 641–648.
Sun, C., Lee, C.-T.A., 2022. Redox evolution of crystallizing magmas with CHOS volatiles and its implications for atmospheric oxygenation. Geochimica et Cosmochimica Acta 338, 302–321.
Sun, C., Yao, L., 2024. Redox equilibria of iron in low- to high-silica melts: A simple model and its applications to C-H-O-S degassing. Earth and Planetary Science Letters 638.
Tang, M., Erdman, M., Eldridge, G., Lee, C.-T.A., 2018. The redox "filter" beneath magmatic orogens and the formation of continental crust. Science Advances 4.
Tang, M., Guo, Z., Cao, W., Chu, X., 2024a. Revisiting zircon Eu anomaly as a proxy for crustal thickness: A case study of the Sierra Nevada Batholith. Earth and Planetary Science Letters 643.
Tang, M., Ji, W.-Q., Chu, X., Wu, A., Chen, C., 2021. Reconstructing crustal thickness evolution from europium anomalies in detrital zircons. Geology 49, 76–80.
Tang, M., Lee, C.-T.A., Costin, G., Höfer, H.E., 2019. Recycling reduced iron at the base of magmatic orogens. Earth and Planetary Science Letters 528.
Tang, M., Lee, C.-T.A., Ji, W.-Q., Wang, R., Costin, G., 2020. Crustal thickening and endogenic oxidation of magmatic sulfur. Science Advances 6.
Tang, M., Liu, X., Chen, K., 2023. High Mg# of the continental crust explained by calc-alkaline differentiation. National Science Review 10, nwac258.
Tang, M., Wang, J., Lee, C.-T.A., 2024b. Reevaluating the oxidation effect of garnet crystallization. Lithos 470–471.
Wang, Q., Zhu, D.-C., Cawood, P.A., Zhao, Z.-D., Liu, S.-A., Chung, S.-L., Zhang, L.-L., Liu, D., Zheng, Y.-C., Dai, J.-G., 2015a. Eocene magmatic processes and crustal thickening in southern Tibet: Insights from strongly fractionated ca. 43 Ma granites in the western Gangdese Batholith. Lithos 239, 128-141.
Wang, J., Tang, M., Chen, H., Wang, X.-L., Wu, B., 2025a. Sulfur contents in zircon-hosted and separated apatite in Archean TTGs: implications for the redox state of Archean felsic magmas. Geochimica et Cosmochimica Acta.
Wang, J., Xiong, X., Takahashi, E., Zhang, L., Li, L., Liu, X., 2019. Oxidation state of arc mantle revealed by partitioning of V, Sc, and Ti between mantle minerals and basaltic melts. Journal of Geophysical Research: Solid Earth 124, 4617–4638.
Wang, M., Wang, Z., Guo, L., Zou, Z., Wu, F., Dai, W., Guo, J., Chen, K., Feng, L., Chen, H., 2025b. Calcium isotope composition of the Gangdese continental arc deep crust and implications for making continental crust. Geochimica et Cosmochimica Acta.
Wang, R., Richards, J.P., Zhou, L.-m., Hou, Z.-q., Stern, R.A., Creaser, R.A., Zhu, J.-j., 2015b. The role of Indian and Tibetan lithosphere in spatial distribution of Cenozoic magmatism and porphyry Cu–Mo deposits in the Gangdese belt, southern Tibet. Earth-Science Reviews 150, 68–94.
Waters, L.E., Lange, R.A., 2016. No effect of H2O degassing on the oxidation state of magmatic liquids. Earth and Planetary Science Letters 447, 48–59.
Wittlinger, G., Farra, V., Hetényi, G., Vergne, J., Nábělek, J., 2009. Seismic velocities in Southern Tibet lower crust: a receiver function approach for eclogite detection. Geophysical Journal International 177, 1037–1049.
Xu, Q., Ding, L., Cao, Y., Cai, F., Li, S., Tan, X., Kershaw, S., Tang, H., 2023. Late Cretaceous–early Paleogene rise of the Gangdese magmatic arc (south Tibet) from sea level to high mountains. Bulletin 135, 1939–1954.
Xu, Q., Zhao, J., Yuan, X., Liu, H., Pei, S., 2015. Mapping crustal structure beneath southern Tibet: Seismic evidence for continental crustal underthrusting. Gondwana Research 27, 1487–1493.
Yin, A., Harrison, T.M., 2000. Geologic evolution of the Himalayan-Tibetan orogen. Annual review of earth and planetary sciences 28, 211–280.
Zhang, J., Wang, R., Hong, J., 2022. Amphibole fractionation and its potential redox effect on arc crust: Evidence from the Kohistan arc cumulates. American Mineralogist 107, 1779–1788.
Zhu, D.-C., Wang, Q., Weinberg, R.F., Cawood, P.A., Zhao, Z., Hou, Z.-Q., Mo, X.-X., 2023. Continental Crustal Growth Processes Recorded in the Gangdese Batholith. Southern Tibet. Annual Review of Earth and Planetary Sciences 51, 155–188.
Zhu, D.C., Wang, Q., Cawood, P.A., Zhao, Z.D., Mo, X.X., 2017. Raising the Gangdese Mountains in southern Tibet. Journal of Geophysical Research: Solid Earth 122, 214–223.